SCIENTIFIC REPORTS

OPEN

SUBJECT AREAS:
NANOPARTICLES
NANOSCALE MATERIALS

Received
22 November 2013

Accepted
20 January 2014

Published
11 February 2014

Correspondence and requests for materials should be addressed to Y.Q.L. (yqli@suda.edu.cn) or M.W.S. (mwshao@suda.edu.cn)

The Effect of Dielectric Constants on Noble Metal/Semiconductor SERS Enhancement: FDTD Simulation and Experiment Validation of Ag/Ge and Ag/Si Substrates

Tao Wang[1,2], Zhaoshun Zhang[1], Fan Liao[1], Qian Cai[1], Yanqing Li[1], Shuit-Tong Lee[1] & Mingwang Shao[1]

[1]Institute of Functional Nano and Soft Materials (FUNSOM), Jiangsu Key Laboratory for Carbon-based Functional Materials and Devices & Collaborative Innovation Center of Suzhou Nano Science and Technology, Soochow University, Suzhou, Jiangsu 215123, P. R. China, [2]Anhui Key Laboratory of Functional Coordination Compounds, Anqing Normal University, Anqing 246011, People's Republic of China.

The finite-difference time-domain (FDTD) method was employed to simulate the electric field distribution for noble metal (Au or Ag)/semiconductor (Ge or Si) substrates. The simulation showed that noble metal/Ge had stronger SERS enhancement than noble metal/Si, which was mainly attributed to the different dielectric constants of semiconductors. In order to verify the simulation, Ag nanoparticles with the diameter of ca. 40 nm were grown on Ge or Si wafer (Ag/Ge or Ag/Si) and employed as surface-enhanced Raman scattering substrates to detect analytes in solution. The experiment demonstrated that both the two substrates exhibited excellent performance in the low concentration detection of Rhodamine 6G. Besides, the enhancement factor (1.3×10^9) and relative standard deviation values (less than 11%) of Ag/Ge substrate were both better than those of Ag/Si (2.9×10^7 and less than 15%, respectively), which was consistent with the FDTD simulation. Moreover, Ag nanoparticles were grown *in-situ* on Ge substrate, which kept the nanoparticles from aggregation in the detection. To data, Ag/Ge substrates showed the best performance for their sensitivity and uniformity among the noble metal/semiconductor ones.

As a powerful analytical tool, Raman scattering is ideal for detecting and identifying specific targets because of its ability to provide vibrational signatures associated with chemical and structural information of the analyzed object[1–3]. However, Raman scattering is very weak due to the small cross-section of molecules. The surface enhanced Raman scattering (SERS) effect can overcome this drawback and exhibit average enhancement factors (EFs) of $\sim 10^6$ or even greater[4].

SERS-active substrates are key point to improve EF in the SERS detection. Over the past several decades, many techniques have been developed for fabricating the high-performance SERS-active substrates, such as electron beam lithography[5], Langmuir-Blodgett assembly[6], nanosphere lithography[7], self-assembly[8], DNA-assisted[9], and oblique angle deposition[10]. All these methods were valuable. Yet, there existed some advantages: (1) the process was often complex and time-consuming; (2) the SERS substrates with a large area were difficult to fabricate for the limitation of preparation; (3) some complex and expensive instruments were required in the fabrication process, which imposed restriction on the popularity of the substrates. Therefore, it was highly desirable to prepare the high-performance SERS-active substrates by a green, time-saving and high-throughput method.

As to substrate materials, noble metal nanoparticles, such as AuNPs, AgNPs and CuNPs, are widely used in SERS substrates for their capability of efficient SERS effect[11–15]. In addition, noble metal/semiconductor heterojunctions, which have wide applications in nanoelectronics, optoelectronics, plasmonics, medical diagnostics, catalysis, drug delivery, and chemical sensing[16], also have shown effective enhancements in Raman scattering and were demonstrated to be appropriate as versatile SERS substrates[17,18]. Peng *et al.* synthesized AgNP/GeNW substrate from the reaction of HF-etched GeNWs and silver nitrate[19]; Yin *et al.* prepared AgNP/ZnO hollow

Table 1 | The maximum intensity ($\langle|E|^2\rangle$) of the noble metal/semiconductor substrates and their ratios

	Au/Ge	Au/Si	R_1	Ag/Ge	Ag/Si	R_2
514 nm	82.5	67.8	1.22	123	88	1.40
633 nm	63	55.8	1.13	30.3	26.6	1.14

R_1 is the maximum intensity ratio between Au/Ge and Au/Si.
R_2 is the maximum intensity ratio between Ag/Ge and Ag/Si.

nanosphere arrays using self-assembled monolayer polystyrene nanospheres as the template[20]; Li *et al.* deposited the Au particles onto the TiO_2 surface using photocatalytic deposition and a hydrothermal method[21].

In comparison with single metal clusters, noble metal/semiconductor heterojunctions had some advantages: firstly, the semiconductors provided supports to the noble metals and prevented the small nanoparticles from aggression, which was essential to the obtainment of stable and reproducible SERS signals; Secondly, it was beneficial for surface plasmon coupling when the noble metals cooperated with semiconductors[22,23]; For example, the LSPR of Ag particles on ZnO could be generated under laser irradiation to improve the SERS signals[24]. The previous reports also demonstrated that the electron transfer from the semiconductor to the metal through the interface of heterojunction could further improve the SERS enhancement effect[25] and some SERS substrate based on metal/semiconductor were recyclable[26,27].

Although the substrates mentioned above could get high sensitivity SERS signals, their uniformity and reproducibility still needed to improve. In order to get qualified SERS substrate, our group has investigated CuNPs/Si substrate with high sensitivity and reproducibility SERS signals[28]. In the interest of even higher performance of noble metal/semiconductor substrate, we employed the finite-difference time-domain (FDTD) method to search for better noble metal/semiconductor substrates. It is now widely accepted that the SERS enhancement has two mechanisms: electromagnetic (EM) enhancement induced by the surface plasmon resonance and the chemical enhancement (CM) originated from the charge transfer between the metal and the molecule[29,30]. The EM mechanism contributes to an enhancement factor of more than 10^6 or even to single molecule detection while CM mechanism could enhance up to 10–100. FDTD simulation is a numerical technique for Maxwell's equations and mainly focuses on EM mechanism.

FDTD is a powerful for modeling computational electrodynamics, which is an important related parameter to SERS intensity[31–33]. Ge was chosen because it is also an important semiconductor[34]. The electric field intensities were simulated by assumption same diameter noble metal nanoparticles (Au or Ag) decorated on Ge or Si wafer, respectively. The simulation clearly showed that the maximum electric field intensity of noble metal/Ge substrate was the larger one.

Ag/Ge and Ag/Si substrates were chosen in the experiments to verify the theoretical simulation. The Ag nanoparticles (NPs) were grown on the Ge or Si wafer by solution methods, which were served as SERS substrates in the detection of Rhodamine 6G (R6G) and 4-mercaptobenzoic acid (MBA). Both substrates showed high sensitivity and reproducibility of the Raman signals in SERS detection. Moreover, the enhancement factor (1.3×10^9) and relative standard deviation values (less than 11%) of Ag/Ge substrate were both better than those of Ag/Si (2.9×10^7 and less than 15%, respectively), which was consistent with the FDTD simulation.

In addition to the advantages in the sensitivity and uniformity, Ag/Ge substrate could be fabricated with a green method: only two pollution-free ingredients, silver nitrate and germanium, were employed, while hydrofluoric acid was used for Ag/Si.

Results

The FDTD simulation for noble metal/semiconductor substrates. Intensity ($\langle|E|^2\rangle$) distributions obtained from 3D FDTD calculations based on the following parameters: the diameter of noble metal NPs was 40 nm with interparticle gap of 5 nm placing on Ge or Si wafer; two incident laser wavelengths (514 and 633 nm) were chosen. The detailed process was illustrated in Figure S1 (Supporting information). The maximum intensity ($\langle|E|^2\rangle$) of each noble metal/semiconductor was listed in Table 1.

It is well known that the Raman scattering efficiency is inversely proportional to fourth power of the wavelength of incident laser and the short-wavelength laser may obtain strong Raman signals[35]. So the maximum intensity of the substrates with a 514-nm laser was higher than that with 633 nm.

It also can be found that the maximum intensity ($\langle|E|^2\rangle$) of the substrates with Ge was larger than those with Si. Take Ag/Ge and Ag/Si at the wavelength of 633 nm as example. The simulation was depictured in Figure 1. The maximum intensity ($\langle|E|^2\rangle$) of Ag/Ge was 30.3, while that of Ag/Si was 26.6. As the SERS signals were proportional to the value ($\langle|E|^2\rangle$), the Ag/Ge substrate obviously has larger SERS enhancement than Ag/Si substrate. Moreover, the value is much larger than that of one Ag nanoparticle on Ge wafer, which is only 2.9 (Figure S2). It means that the hotspot is formed between the two Ag nanoparticles and giant SERS enhancement can be obtained.

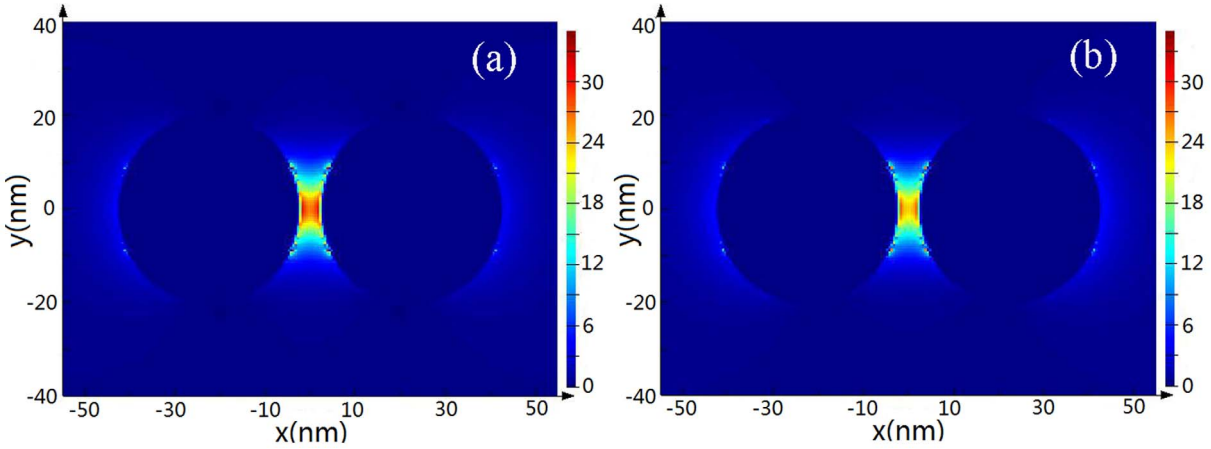

Figure 1 | Intensity ($\langle|E|^2\rangle$) distributions obtained from 3D FDTD calculations at wavelength 633 nm of silver nanoparticles, with 40 nm diameter and interparticle separation of 5 nm, on (a) Ge wafer and (b) Si wafer.

Table 2 | Dielectric constants of Ge and Si at 514 nm and 633 nm

	Ge		Si	
	Real part	Imaginary part	Real part	Imaginary part
514 nm	14.893	22.41	17.865	0.507
633 nm	29.294	9.161	15.064	0.147

Why these two substrates had such a large difference in intensity? The reason can be ascribed to the different properties of Si and Ge considering that the other simulation parameters were the same. In the FDTD simulation, the dielectric constants of Si and Ge were involved. Ge has much larger imaginary part of dielectric constants than Si as shown in Table 2, which caused stronger interaction between Ag and Ge and led to stronger localized plasmon resonance on Ag/Ge substrate.

From the above discussions, all of our simulations were consistent with the previous reports, which also indicated that the materials with high imaginary part of dielectric constants were in favor of enhancing their interaction to metallic nanoparticles while the real part had only a less significant effect[36–38].

Next, further experimental proof is needed to demonstrate the feasibility of simulation. In order to select an optimal experimental substrate, the intensity values were compared between noble metal/Ge and noble metal/Si. From Table 1, the intensity ratios between Ag/Ge and Ag/Si with incident laser of 514 and 633 nm were both larger than those between Au/Ge and Au/Si.

So, Ag/Ge and Ag/Si were chosen in the experiment because of the larger difference intensity between Ag/Ge and Ag/Si. The Ag nanoparticles (NPs) were grown on the Ge and Si wafer by solution methods. As a newly reported SERS substrate, Ag/Ge was studied in detail below.

Characterization of Ag NPs grown on Ge wafer. The XRD pattern of Ag NPs in situ growing on Ge wafer is shown in Figure S3. In addition to the diffraction peak of Ge and GeO2, the peaks centered at 38.1 and 44.3° may be indexed as (111) and (200) crystal planes of cubic Ag (JCPDS. 04-0783).

The formation process of high quality Ag NPs is strongly dependent on the reaction conditions. The SEM images of Ag/Ge prepared by $AgNO_3$ with different concentration for different reaction time are shown in Figure S4. And Figure 2 shows the SEM images of Ag NPs growing on Ge wafer under optimal condition. The low magnification image (Figure 2a) reveals a large scale and irregular Ag NPs. And the high magnification one (Figure 2b) shows that most of these Ag NPs are irregular with the diameter of ca. 40 nm (Figure S5).

Detailed information about the surface electronic structure of the obtained substrate was provided by the XPS analysis. Figure 3a shows the XPS spectrum of Ag 3d of the Ag NPs. The binding energies of Ag $3d_{5/2}$ and Ag $3d_{3/2}$ are at 368.3 and 374.3 eV, which are consistent with those of Ag metal[39] and the Ag NPs on Ge prepared via the block copolymer mediated method[40], confirming that they are Ag NPs on the surface of Ge wafer. The XPS spectrum of Ge 3d (Figure 3b) has established that the surface Ge can be readily oxidized by electronegative elements through several oxidation state (+1 – +4), and the binding energy increase associated with an unit increase in oxidation state (i.e., per Ge-O bond) is ~0.85 eV)[41]. The peak at 33.3 eV thus is attributed to GeO_2 on the surface of Ge wafer. The binding energies of Ge $3d_{5/2}$ and Ge $3d_{3/2}$ are 30.2 and 30.8 eV due to spin – orbit splitting.

The formation of Ag NPs on Ge wafer is illustrated in Figure 4: the Ge wafer contacting with $AgNO_3$ solution immediately initiates the rapid reduction of Ag^+ ions by surface electrons, resulting in the formation of small Ag nanocrystals (Figure 4a). Once the nuclei are formed and the surface electrons are expended, hole injection process dominates the growth of the Ag particles because the equilibrium potential (≥4.885 eV for $AgNO_3$ solutions with concentrations higher than 1×10^{-7} M) of Ag^+/Ag couple overlaps the valence band (with band edge of 4.0 eV) of Ge (Figure 4b). As shown in Figure 4c, when a Ag^+ ion reaches the surface of a Ag nucleus, it releases a hole and becomes a Ag atom. The released hole migrates to the Ag/Ge interface through the Ag nucleus, and then diffuses in the Ge lattice to react with surface Ge in the presence of water. The reaction results in the production of GeO_2, which can be dissolved in water, making new Ge surface exposed to Ag^+, and grow new Ag NPs. The chemical reaction equation is:

$$4AgNO_3 + Ge + 2H_2O \rightarrow 4Ag + GeO_2 + 4HNO_3 \quad (1)$$

SERS of Ag NPs grown on Ge wafer. In order to evaluate the SERS of the substrate, Raman spectra were collected employing R6G as the probe molecule owing to its well-established vibrational features. In water, the resonance Raman enhancement factor of R6G under the 532 nm laser irradiation is $(2.7 \pm 0.3) \times 10^3$, larger than the value under 638 nm laser irradiation (9.18 ± 0.98)[42]. Therefore, it is reasonable to deduce that the 633 nm He-Ne laser was employed in all the Raman detections to reduce the influence of surface-enhanced resonance Raman scattering.

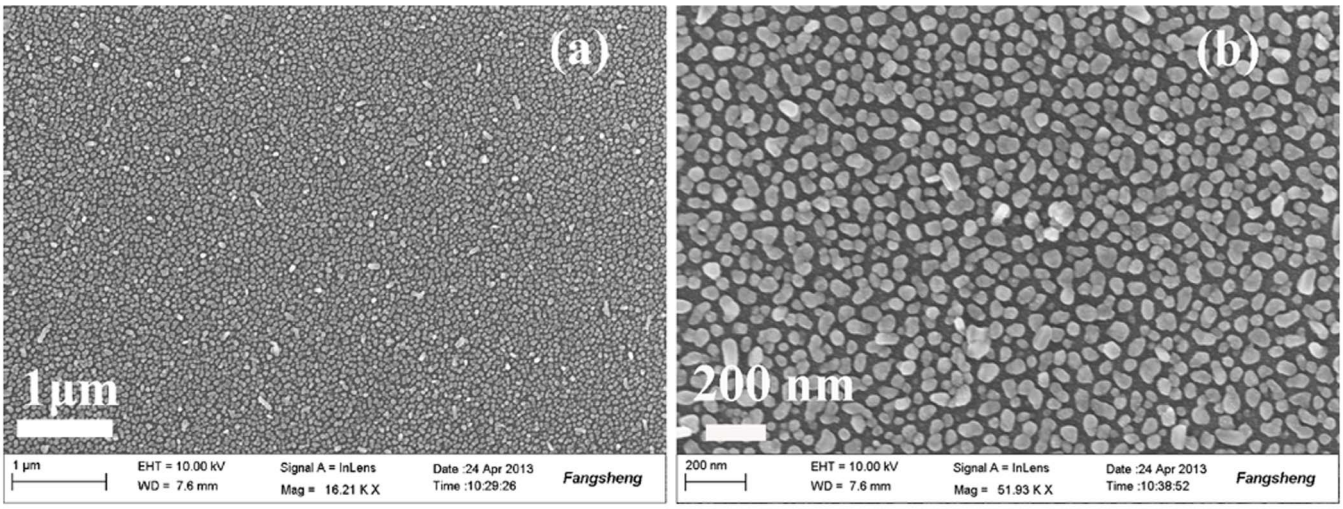

Figure 2 | The SEM images of Ag NPs growing on Ge wafer: (a) in a low magnification, and (b) in a high magnification.

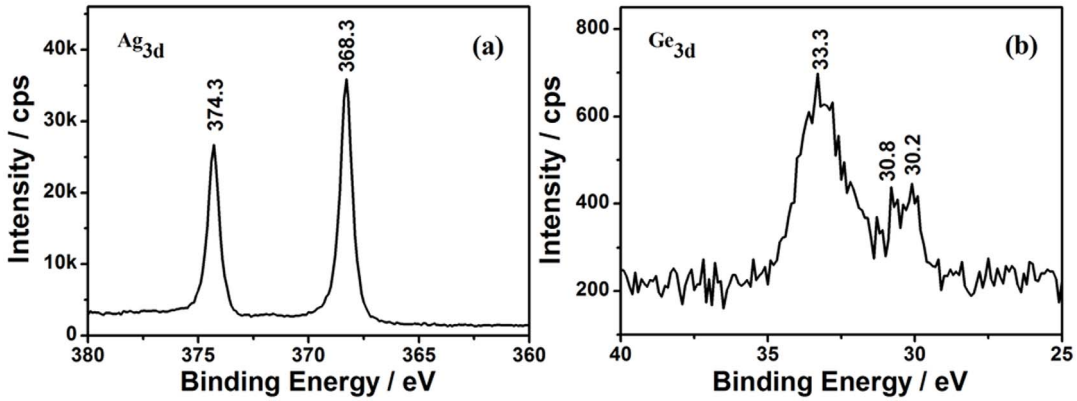

Figure 3 | **The high-resolution XPS spectra of (a) Ag 3 d, and (b) Ge 3 d.**

SERS measurements were conducted as follows. The Ge wafer with Ag NPs was cut into small pieces with the size of 0.5 × 0.5 cm^2, and then placed in a quartz cell of 150 μL with a quartz window. The cell was filled up with 1 × 10^{-10} M R6G aqueous solution, and the distance between the Ge wafer and this quartz window is about 0.5 mm. In the process of Raman detection, the laser was focused on the Ag NPs through the quartz window. The whole SERS detection was illustrate in Figure S6. As we predicted, the substrate exhibited remarkable SERS activity (upper part of Figure 5). The main peaks of R6G's characteristic vibrations in SERS, the strongest bands of carbon skeleton stretching modes at 1366, 1511, 1575, 1651 cm^{-1}, are similar to the normal solution Raman spectrum of R6G in Figure S7. Some bands centered at 1129 and 1605 cm^{-1} were also observed obviously in SERS, which were hardly observed in the normal Raman spectrum. The appearance of these bands further corroborates the excellent enhancement effect of the substrate.

Another critical point shown in the lower part of Figure 5 is the exceptional uniformity of the substrate. The SERS contour was plotted after the line mapping which was measured spot-to-spot at 1 × 10^{-10} M R6G aqueous solution. In all the 200 spots, each spot exhibited a powerful capability to enhance Raman signals of the R6G molecules.

To further semi-quantitatively assess the uniformity of these SERS signals, the relative standard deviation (RSD) of the intensity of the carbon skeleton-stretching modes was calculated. The values of RSD of vibrations at 1314, 1366, 1511, and 1651 cm^{-1} (Figure 6) are 8.87%, 9.32%, 10.93%, and 8.80%, respectively, indicating the high uniformity of the substrate vigorously. Less than 11% of the RSD of the four bands' intensity further demonstrated that the as-prepared substrate was suitable for a highly reproducible SERS substrate[43]. As is shown in Figure S8, the Raman intensities of R6G show a log-normal distribution, indicating that there is a large coverage of SERS hotspots in the scanned area[44,45]. Moreover, the distribution of peaks is narrow and further confirmed the uniformity of SERS substrate. To quantitatively demonstrate the enhancement, the peak at 1511 cm^{-1} was used to calculate the enhancement factor (EF) using Equ. 2[46]:

$$EF = \frac{I_{SERS} N_0}{I_0 N_{SERS}} \quad (2)$$

where N_0 and I_0 are the number of molecules and intensity for regular Raman measurement with 0.01 M R6G solution (Figure S7), respectively; and N_{SERS} and I_{SERS} are the number of molecules and peak intensity for the SERS measurement with 1 × 10^{-10} M R6G solution, respectively. EF was calculated as 1.3 × 10^9 (the details were shown in Supporting Information). The SERS detection in solution could warrant the reproducibility, although the majority was conducted in dry condition. In the literature, Huang *et al.* reported the enhancement factor of 1.6 × 10^5 using Ag colloids to detect R6G[47]. Therefore, these Ag/Ge substrates exhibited excellent sensitivity and uniformity in the SERE detection of analysts in solution.

The SEM image of as-prepared Ag/Si substrate (Figure S9) shows that a large scale Ag NPs with the diameter of ca. 40 nm (Figure S10) were grown on the Si wafer. In the Raman detection of 1 × 10^{-9} M R6G aqueous solution, the as-prepared Ag/Si substrate shows high uniformity (Figure S11). The RSD values of vibrations at 1311, 1363,

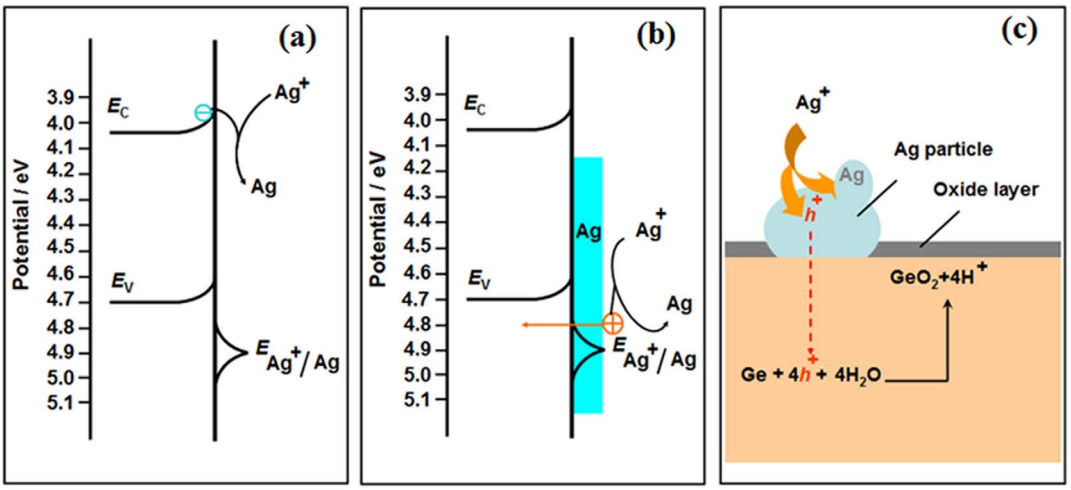

Figure 4 | **Schematic of Ag NPs grown on the Ge wafer.**

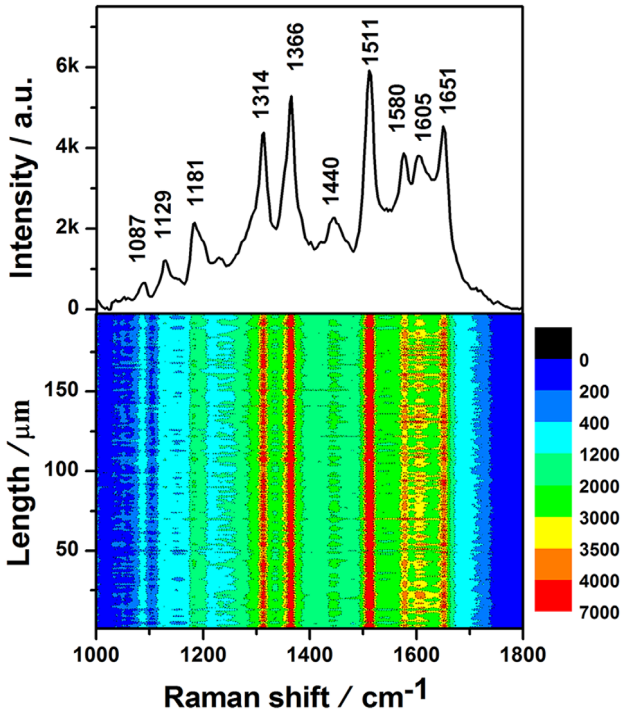

Figure 5 | The Raman spectrum of R6G aqueous solution (1×10^{-10} M) on the as-prepared Ag/Ge substrate (upper part), and the SERS contour (lower part).

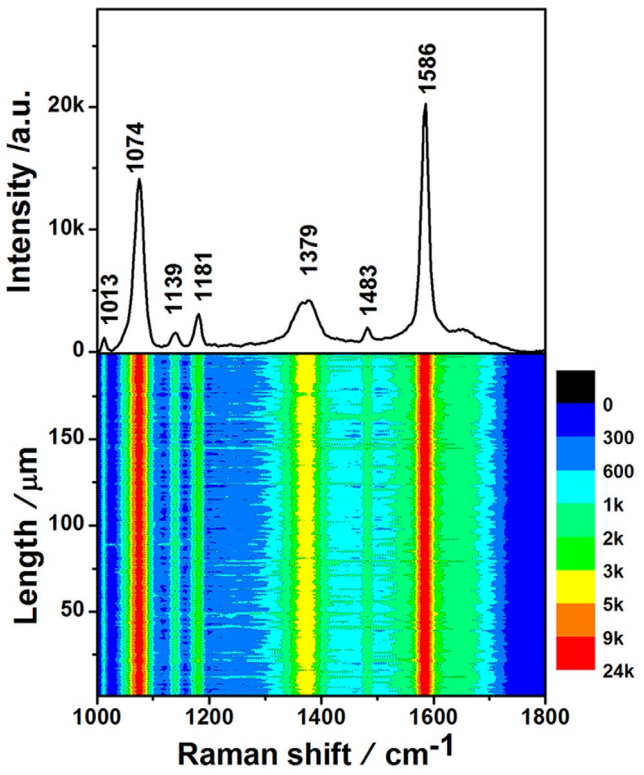

Figure 7 | The Raman spectrum of MBA aqueous solution (at 1×10^{-9} M) on the as-prepared Ag/Ge substrate (upper part), and the SERS contour (lower part).

1512, and 1651 cm^{-1} are 13.96%, 14.45%, 14.90%, and 15.00%, respectively (Figure S12). The Raman intensities of R6G also show a log-normal distribution (Figure S13). However, the EF of the as-prepared Ag/Si is 2.9×10^7 using the similar calculation, which is about 2% of the value resulting from the as-prepared Ag/Ge substrate.

The as-prepared Ag/Ge substrates were also used to detect 1×10^{-9} M MBA aqueous solution. The SERS spectrum from the MBA

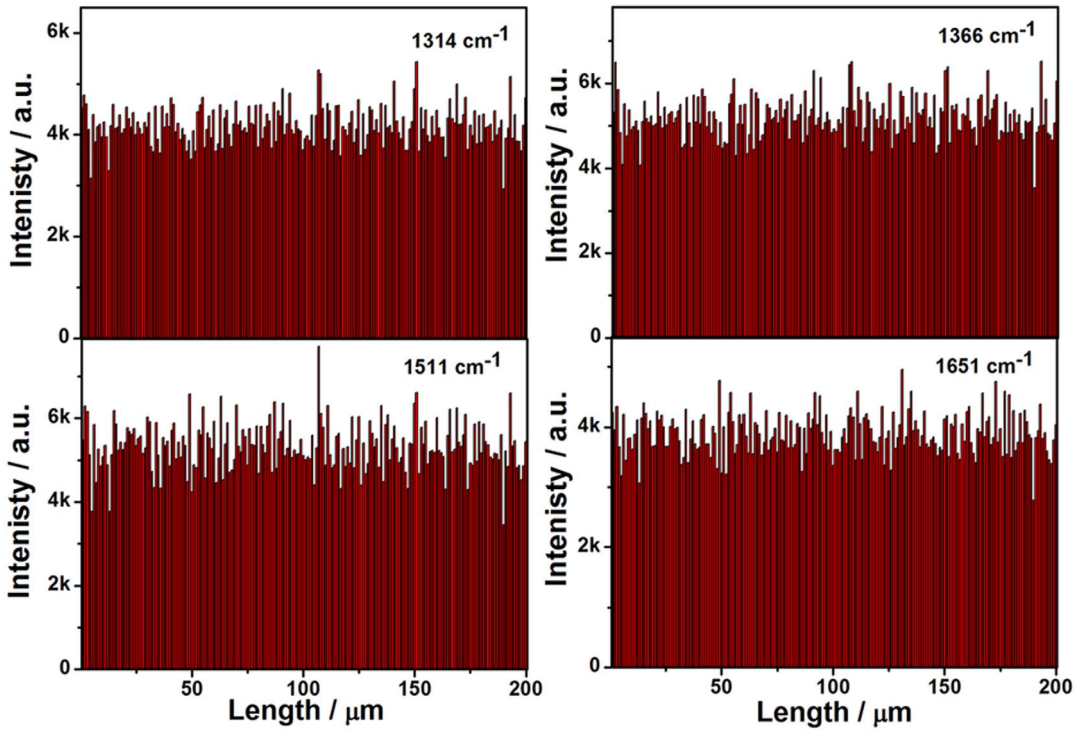

Figure 6 | The intensities of the main Raman vibrations of R6G aqueous solution (1×10^{-10} M) in 200 spots SERS line-scan spectra collected on the as-prepared Ag/Ge substrate.

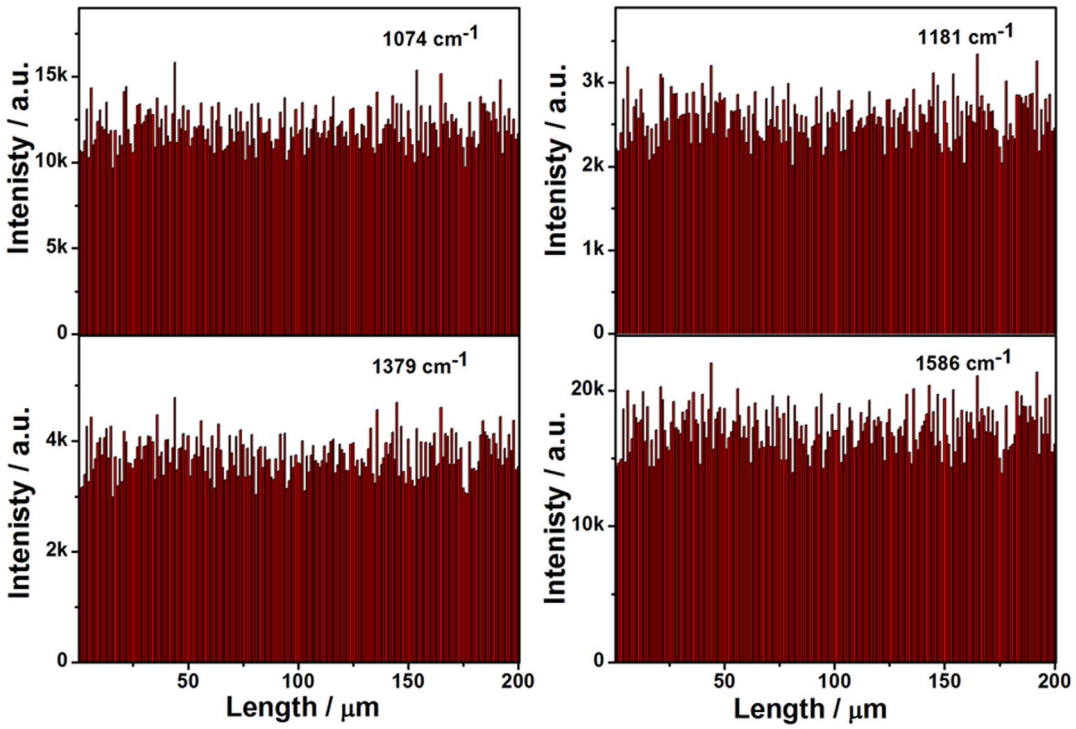

Figure 8 | The intensities of the main Raman vibrations of MBA aqueous solution (at 1×10^{-9} M) in the 200 spots SERS line-scan spectra collected on the as-prepared Ag/Ge substrate.

(Figure 7, upper part) is similar with the normal Raman spectrum of MBA powder (Figure S14) and in good agreement with literatures[48,49]. The SERS contour (Figure 7, lower part) was obtained from the line mapping conducted spot-to-spot on substrate in the 1×10^{-9} M MBA aqueous solution. For all the 200 spots, each spot exhibits the strong SERS signals. The RSD values of vibrations at 1074, 1181, 1379, and 1586 cm^{-1} (Figure 8) are 9.14%, 9.94%, 9.32%, and 9.39%, respectively, which could vigorously indicate the high uniformity of the substrate, further confirming the remarkable enhancement effect and high uniformity of the substrate. As is shown in Figure S15, the Raman intensities of MBA show a log-normal distribution, further indicating that there is a large coverage of SERS hotspots in the scanned area. In addition, the width of their distribution is almost identical to that in the Raman spectra of R6G, demonstrating the good reproducibility of the SERS substrate.

It is worth mention that all the measurements of Raman spectra were conducted in the aqueous solution. It helps to get high uniform and reproducible signals and obtain the real structure information of probe molecules in solution. This is very beneficial to the research on the mechanism of reaction in situ in solution through the Raman measurement.

In addition to the reliable reproducibility and excellent sensitivity, the SERS substrate based on Ag NPs grown on Ge wafer also have the following advantages: first, the surface of Ag NPs was clean, which increases the surface adsorption capacity to target molecules. Secondly, Ag NPs were uniformly distributed on Ge wafer, which ensure the sensitivity and uniformity of the substrates: There were about 300 Ag particles in a square micrometer area, calculated from the SEM image in Figure 2b. The diameter of the laser spot was calculated to be 1.55 μm, according to the Equ. 3[50]:

$$D = 1.22\lambda/N_A \quad (3)$$

where λ is the wavelength of laser used and N_A is the numerical aperture of the objective. The laser spot covered more than 560 Ag NPs ($\pi \times (1.55/2)^2 \times 300 = 563$) and ensured the large electromagnetic field coupling. Thirdly, these Ag NPs were grown and fixed on the Ge wafer, they would keep away from aggregating or growing large to ensure the SERS activity in the Raman detection, while metal NPs without supporting wouldn't.

Discussion

The intensity distributions of noble metal/semiconductor substrates were simulated with the FDTD methods. The simulation reveals that noble metal/Ge substrate has larger electromagnetic field coupling than noble metal/Si, which may attribute to the larger imaginary part of dielectric constants of Ge. Ag/Ge and Ag/Si substrates were fabricated and employed in SERS detection to verify the simulation. The SERS signals collected on Ag/Ge in the dilute R6G and MBA solution showed larger enhancement and higher uniformity than those on Ag/Si. Moreover, the Ag nanoparticles were grown in-situ on Ge substrate, which kept the nanoparticles from aggregation in the detection. To date, Ag/Ge substrates showed the best performance for their sensitivity and uniformity among the noble metal/semiconductor ones.

Even more to the point, the preparation process of Ag/Ge was a green one. In a word, we believe that combining theoretical simulation and experimental detection will help to find high sensitive and excellent reproducible SERS substrates for practical applications in the future.

Methods

Synthesis and characterization. All chemical reagents were of analytical grade, which were purchased from Shanghai Chemical Company and used without further purification. The water used was doubly distilled water. Ge (100) wafers (n type, 0.01 Ω·cm) with a diameter of 50 mm and a thickness of 0.5 mm were purchased from Hefei Kejing Materials S2 Technology Co., Ltd (China).

The Ge wafer was cleaned following the previously reported process[51]. After dried with nitrogen, the Ge wafer was immediately immersed in 300 ml 1×10^{-4} M silver nitrate solution for 10 min and taken out. Then, it was rinsed with deionized water and ethanol sequentially, and dried with nitrogen gas at once. Several contrast tests of different concentration and different reaction time (1×10^{-5} M $AgNO_3$ for 20 min; 1×10^{-4} M $AgNO_3$ for 20 min; 1×10^{-3} M $AgNO_3$ for 10 min and 1×10^{-2} M $AgNO_3$ for 10 min) were also conducted.

The Si wafers were cut to a size of 1 × 1 cm and cleared sequentially with acetone, ethanol, H_2SO_4/H_2O_2, and water. After dried with nitrogen, the cleared Si wafers were placed in the 10% HF solution for just 1 s, then quickly placed in the mixture solution containing 6 mL 1×10^{-2} M $AgNO_3$ and 4 mL 4% HF for just 3 s. After that the Si wafers covered with Ag NPs were taken out, rinsed with distilled water, and dried at room temperate.

The wafer grown with Ag NPs was characterized via X-ray powder diffraction (XRD), which was carried out on a Philips X'pert PRO MPD diffractometer with Cu Kα radiation (λ = 0.15406 nm). The morphologies of Ag NPs formed on the Ge wafer were performed on a Zeiss Supra 55 field scanning electron microscopy (SEM) operating in high vacuum mode at 10 kV accelerating voltages. The energy dispersive X-ray analysis (EDS) spectroscopy was taken on a FEI-quanta 200 scanning electron microscope with acceleration voltage of 30 kV. The surface state of SERS substrate was studied by XPS measurement (Kratos AXIS UltraDLD ultrahigh vacuum surface analysis system) with Al Kα radiation (1486 eV) as probe. An electron flood gun was employed for all measurements to compensate charging, and final spectra were calibrated to the adventitious carbon C 1 s peak at 284.6 eV.

Finite-difference time domain (FDTD) simulations. 3D FDTD simulations (Lumerical Solutions Ltd.) were used to determine the near-field intensities around the silver nanoparticles grown over the Ge or Si substrate. Electromagnetic field distribution was calculated for silver nanoparticles with a diameter of 40 nm and interparticle separation of 5 nm, on Ge or Si wafer. A plane wave polarized light of wavelength 633 nm was used along the z-axis. For minimum simulation time and to maximize field enhancement resolution, the mesh override region was set to 0.5 nm, and the overall simulation time as 500 fs.

Raman microscopy. An HR 800 Raman spectroscopy (J Y, France) equipped with a synapse CCD detector and a confocal Olympus microscope was used to collect Raman spectra. SERS experiments were conducted in the line-mapping mode and 1 μm increment using R6G aqueous solution as model molecules. The spectrograph used 600 g/mm gratings. SERS spectra were collected at LMPlanFl 50 × Objective Lens (lens with the long focal length) with a numerical aperture of 0.50 and the accumulation time of 1 s.

1. Li, J. F. *et al.* Shell-isolated nanoparticle-enhanced Raman spectroscopy. *Nature* **464**, 392–395 (2010).
2. Rycenga, M. X. *et al.* Generation of Hot Spots with Silver Nanocubes for Single-Molecule Detection by Surface-Enhanced Raman Scattering. *Angew. Chem. Int. Ed.* **50**, 5473–5477 (2011).
3. Nie, S. M. & Emery, S. R. Probing Single Molecules and Single Nanoparticles by Surface-Enhanced Raman Scattering. *Science* **275**, 1102–1106 (1997).
4. Tripp, R. A., Dluhy, R. A. & Zhao, Y. P. Novel nanostructures for SERS biosensing. *Nano Today* **3**, 31–37 (2008).
5. David, C., Guillot, N., Shen, H., Toury, T. & de la Chapelle, M. L. SERS detection of biomolecules using lithographed nanoparticles towards a reproducible SERS biosensor. *Nanotechnology* **21**, 475501–475501 (2010).
6. Paczesny, J. *et al.* Three Steps of Hierarchical Self Assembly Toward a Stable and Efficient Surface Enhanced Raman Spectroscopy Platform. *Chem. Mater.* **24**, 3667–3673 (2012).
7. Masson, J. F., Gibson, K. F. & Provencher-Girard, A. Surface-Enhanced Raman Spectroscopy Amplification with Film over Etched Nanospheres. *J. Phys. Chem. C* **114**, 22406–22412 (2010).
8. Cho, W. J., Kim, Y. & Kim, J. K. Ultrahigh-Density Array of Silver Nanoclusters for SERS Substrate with High Sensitivity and Excellent Reproducibility. *Acs Nano* **6**, 249–255 (2012).
9. Zheng, Y. *et al.* DNA-Directed Self-Assembly of Core-Satellite Plasmonic Nanostructures: A Highly Sensitive and Reproducible Near-IR SERS Sensor. *Adv. Funct. Mater.* **23**, 1519–1526 (2013).
10. Liu, Y. J., Chu, H. Y. & Zhao, Y. P. Silver Nanorod Array Substrates Fabricated by Oblique Angle Deposition: Morphological, Optical, and SERS Characterizations. *J. Phys. Chem. C* **114**, 8176–8183 (2010).
11. Li, J. F. *et al.* Surface analysis using shell-isolated nanoparticle-enhanced Raman spectroscopy. *Nat. Protoc.* **8**, 52–65 (2013).
12. Que, R. H. *et al.* Highly Reproducible Surface-Enhanced Raman Scattering on a Capillarity-Assisted Gold Nanoparticle Assembly. *Adv. Funct. Mater.* **21**, 3337–3343 (2011).
13. Tian, C. F. *et al.* Nanoparticle Attachment on Silver Corrugated-Wire Nanoantenna for Large Increases of Surface-Enhanced Raman Scattering. *Acs Nano* **5**, 9442–9449 (2011).
14. Liu, J. W. *et al.* Ordering Ag nanowire arrays by a glass capillary: A portable, reusable and durable SERS substrate. *Sci. Rep.* **2**, 987; doi:10.1038/srep00987 (2012).
15. Chen, L. Y., Yu, J. S., Fujita, T. & Chen, M. W. Nanoporous Copper with Tunable Nanoporosity for SERS Applications. *Adv. Funct. Mater.* **19**, 1221–1226 (2009).
16. Feng, X., Hu, G. & Hu, J. Solution-phase synthesis of metal and/or semiconductor homojunction/heterojunction nanomaterials. *Nanoscale* **3**, 2099–2117 (2011).
17. Ding, X. *et al.* Highly Sensitive SERS Detection of Hg(2+) Ions in Aqueous Media Using Gold Nanoparticles/Graphene Heterojunctions. *ACS Appl. Mater. Interfaces* **5**, 7072–7078 (2013).
18. Chen, L. *et al.* ZnO/Au Composite Nanoarrays As Substrates for Surface-Enhanced Raman Scattering Detection. *J. Phys. Chem. C* **114**, 93–100 (2009).
19. Peng, M. F. *et al.* Reductive Self-Assembling of Ag Nanoparticles on Germanium Nanowires and Their Application in Ultrasensitive Surface-Enhanced Raman Spectroscopy. *Chem. Mater.* **23**, 3296–3301 (2011).
20. Yin, J. *et al.* Ag nanoparticle/ZnO hollow nanosphere arrays: large scale synthesis and surface plasmon resonance effect induced Raman scattering enhancement. *J. Mater. Chem.* **22**, 7902–7909 (2012).
21. Li, X. H., Chen, G. Y., Yang, L. B., Zhen, J. & Liu, J. H. Multifunctional Au-Coated TiO_2 Nanotube Arrays as Recyclable SERS Substrates for Multifold Organic Pollutants Detection. *Adv. Funct. Mater.* **20**, 2815–2824 (2010).
22. Cushing, S. K. *et al.* Photocatalytic Activity Enhanced by Plasmonic Resonant Energy Transfer from Metal to Semiconductor. *J. Am. Chem. Soc.* **134**, 15033–15041 (2012).
23. Ye, L. *et al.* Two Different Roles of Metallic Ag on Ag/AgX/BiOX (X = Cl, Br) Visible Light Photocatalysts: Surface Plasmon Resonance and Z-Scheme Bridge. *ACS Catal.* **2**, 1677–1683 (2012).
24. Song, W., Wang, Y., Hu, H. & Zhao, B. Fabrication of surface-enhanced Raman scattering-active ZnO/Ag composite microspheres. *J. Raman Spectrosc.* **38**, 1320–1325 (2007).
25. Lahiri, A., Wen, R., Kuimalee, S., Kobayashi, S. I. & Park, H. One-step growth of needle and dendritic gold nanostructures on silicon for surface enhanced Raman scattering. *CrystEngComm* **14**, 1241–1246 (2012).
26. Sinha, G., Depero, L. E. & Alessandri, I. Recyclable SERS Substrates Based on Au-Coated ZnO Nanorods. *ACS Appl. Mater. Interfaces* **3**, 2557–2563 (2011).
27. Chen, Y. *et al.* In situ controlled growth of well-dispersed gold nanoparticles in TiO2 nanotube arrays as recyclable substrates for surface-enhanced Raman scattering. *Dalton Trans.* **41**, 1020–1026 (2012).
28. Shao, Q., Que, R. H., Shao, M. W., Chen, L. & Lee, S. T. Copper Nanoparticles Grafted on a Silicon Wafer and Their Excellent Surface-Enhanced Raman Scattering. *Adv. Funct. Mater.* **22**, 2067–2070 (2012).
29. Jayawardhana, S., Rosa, L., Juodkazis, S. & Stoddart, P. R. Additional enhancement of electric field in surface-enhanced Raman Scattering due to Fresnel mechanism. *Sci. Rep.* **3**, 2335 (2013).
30. Tong, L., Zhu, T. & Liu, Z. Approaching the electromagnetic mechanism of surface-enhanced Raman scattering: from self-assembled arrays to individual gold nanoparticles. *Chem. Soc. Rev.* **40**, 1296–1304 (2011).
31. Wells, S. M., Merkulov, I. A., Kravchenko, I. I., Lavrik, N. V. & Sepaniak, M. J. Silicon Nanopillars for Field-Enhanced Surface Spectroscopy. *Acs Nano* **6**, 2948–2959 (2012).
32. Xu, L. *et al.* Regiospecific Plasmonic Assemblies for *in Situ* Raman Spectroscopy in Live Cells. *J. Am. Chem. Soc.* **134**, 1699–1709 (2011).
33. Yoon, I. *et al.* Single Nanowire on a Film as an Efficient SERS-Active Platform. *J. Am. Chem. Soc.* **131**, 758–762 (2008).
34. Hu, W. B. *et al.* Ge-on-Si for Si-based integrated materials and photonic devices. *Front. Optoelectron.* **5**, 41–50 (2012).
35. Lewis, I. R. & Edwards, H. G. M. *Handbook of Raman Spectroscopy: From the research laboratory to the process line.* Ch.2 (Marcel Dekker, Inc., New York 2001).
36. Hutter, T., Elliott, S. R. & Mahajan, S. Interaction of metallic nanoparticles with dielectric substrates: effect of optical constants. *Nanotechnology* **24**, 035201 (2013).
37. Noguez, C. Surface Plasmons on Metal Nanoparticles: The Influence of Shape and Physical Environment. *J. Phys. Chem. C* **111**, 3806–3819 (2007).
38. Wu, Y. P. & Nordlander, P. Finite-Difference Time-Domain Modeling of the Optical Properties of Nanoparticles near Dielectric Substrates. *J. Phys. Chem. C* **114**, 7302–7307 (2010).
39. Chastain, J. *Handbook of X-ray Photoelectron Spectroscopy* (Perkin-Elmer Co., Minnesota 1991).
40. Aizawa, M. & Buriak, J. M. Block Copolymer Templated Chemistry for the Formation of Metallic Nanoparticle Arrays on Semiconductor Surfaces. *Chem. Mater.* **19**, 5090–5101 (2007).
41. Schmeisser, D. *et al.* Surface oxidation states of germanium. *Surf. Sci.* **172**, 455–465 (1986).
42. Ameer, F. S., Pittman, C. U. & Zhang, D. Quantification of Resonance Raman Enhancement Factors for Rhodamine 6G (R6G) in Water and on Gold and Silver Nanoparticles: Implications for Single-Molecule R6G SERS. *J. Phys. Chem. C* **117**, 27096–27104 (2013).
43. Natan, M. J. Concluding Remarks: Surface enhanced Raman scattering. *Faraday Discuss.* **132**, 321–328 (2006).
44. Im, H. *et al.* Self-Assembled Plasmonic Nanoring Cavity Arrays for SERS and LSPR Biosensing. *Adv. Mater.* **25**, 2678–2685 (2013).
45. dos Santos, D. P., Andrade, G. F. S., Temperini, M. L. A. & Brolo, A. G. Electrochemical Control of the Time-Dependent Intensity Fluctuations in Surface-Enhanced Raman Scattering (SERS). *J. Phys. Chem. C* **113**, 17737–17744 (2009).
46. Lu, L. Q., Zheng, Y., Qu, W. G., Yu, H. Q. & Xu, A. W. Hydrophobic Teflon films as concentrators for single-molecule SERS detection. *J. Mater. Chem.* **22**, 20986–20990 (2012).
47. Ciou, S. H., Cao, Y. W., Huang, H. C., Su, D. Y. & Huang, C. L. SERS Enhancement Factors Studies of Silver Nanoprism and Spherical Nanoparticle Colloids in The Presence of Bromide Ions. *J. Phys. Chem. C* **113**, 9520–9525 (2009).

48. Yan, J. *et al.* Highly Sensitive Surface-Enhanced Raman Spectroscopy (SERS) Platforms Based on Silver Nanostructures Fabricated on Polyaniline Membrane Surfaces. *ACS Appl. Mater. Interfaces* **4**, 2752–2756 (2012).
49. Jiang, X. *et al.* Surface-Enhanced Raman Scattering from Synergistic Contribution of Metal and Semiconductor in TiO_2/MBA/Ag(Au) and Ag(Au)/MBA/TiO_2 Assemblies. *J. Phys. Chem. C* **116**, 14650–14655 (2012).
50. Nakashima, S. & Hangyo, M. Characterization of semiconductor materials by Raman microprobe. *IEEE J. Quantum Electron.* **25**, 965–975 (1989).
51. Sayed, S. Y. & Buriak, J. M. Epitaxial Growth of Nanostructured Gold Films on Germanium via Galvanic Displacement. *ACS Appl. Mater. Interfaces* **2**, 3515–3524 (2010).

Acknowledgments

This work was supported by the National Basic Research Program of China (973 Program) (Grant No. 2010CB934502), the National Natural Science Foundation of China (91027041, 61107022), the Priority Academic Program Development of Jiangsu Higher Education Institutions, Innovative Research Teams of Jiangsu Higher Education Institutions and SUN-WIN joint project.

Author contributions

M.S. and Y.L. conceived the experiments. M.S., Y.L. and T.W. wrote the paper. T.W. and F.L. performed the experiments. Q.C. helped to do the experiments. Z.Z. performed FDTD calculations. S.L. gave scientific advice. All authors contributed to the analysis of this manuscript and reviewed the manuscript.

Additional information

Supplementary information accompanies this paper at http://www.nature.com/scientificreports

Competing financial interests: The authors declare no competing financial interests.

How to cite this article: Wang, T. *et al.* The Effect of Dielectric Constants on Noble Metal/Semiconductor SERS Enhancement: FDTD Simulation and Experiment Validation of Ag/Ge and Ag/Si Substrates. *Sci. Rep.* **4**, 4052; DOI:10.1038/srep04052 (2014).